Online Supplemental Material

1) Fourier analysis of mitochondrial size (contains Figures S1 and S2, a–f).

2) Mitochondrial membrane potential: effect of hypoxia/reoxygenation (contains Figure S3).

3) The role of the mitoK_{ATP} in protection signaling (contains Figures S4 and S5).

(4) Additional agents affecting protection; memory-associated versus memory-lacking protection signaling (contains Figures S6 and S7).

5) Effect of intracellular Ca^{2+} concentration on MPT induction in intact cardiac myocytes (contains Figures S8–S11).

SUPPLEMENT 1

Fourier analysis of mitochondrial size

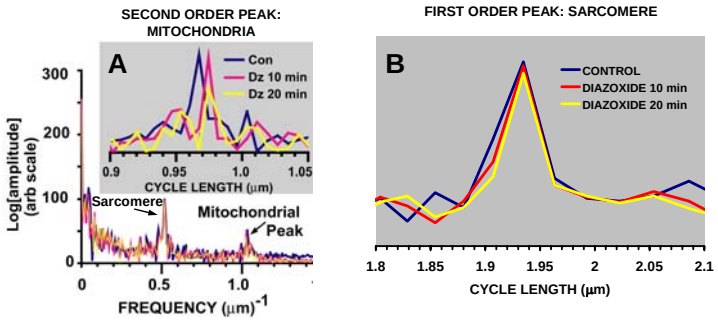

Figure S1. Fourier analysis of mitochondrial size

Cardiac myocytes are composed of regular parallel arrays of myofilaments (divided into repeated series of sarcomere structures with a frequency of ~1.9-1.95 μm along the long axis) alternating with rows of mitochondria (organized at 2 per sarcomere). The optical contrast provided by the various structures comprising the sarcomere and the mitochondria leads to a visible periodic lattice (with ~1.9-1.95 μm and ~0.95-1 μm structures, respectively, along the long axis) that can be analyzed by examining the amplitude of respective peaks in the frequency spectrum obtained from the Fourier series representation of the periodic information contained in images from the cell. Transmitted optics linescan imaging (using a 633 nm laser, scanning 14.1 pixels/μm along the cell long axis for 72.6 or 145.1 μm) was performed to assess changes in mitochondrial volume. Fourier analysis (ImageJ, W. Rasband, NIH, Bethesda, Maryland, USA) of repeating intensity of the linescan

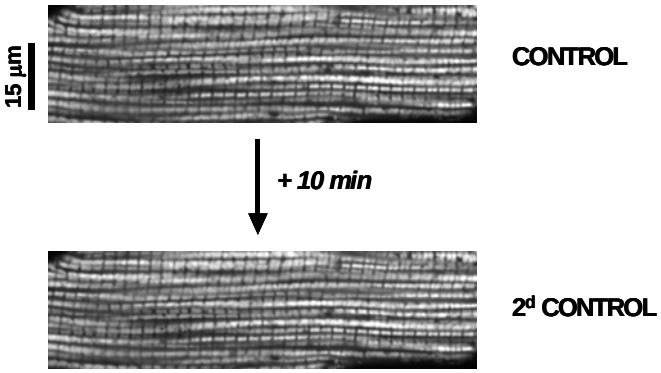

Figure S2a. Consecutive images of TMRM-loaded cardiac myocyte for Fourier analysis of mitochondrial size.

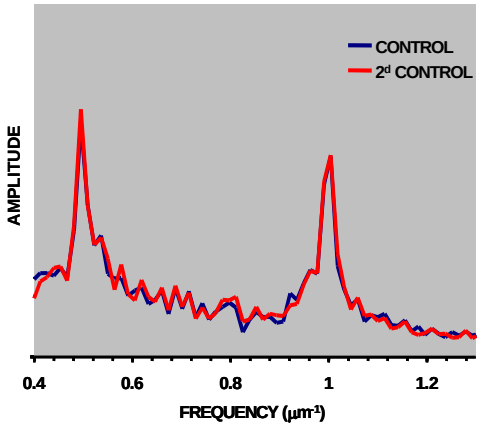

Figure S2b. Fourier analysis of mitochondrial size from TMRM loading: control exposure.

image provided the long-axis spacing of the sarcomere and mitochondrial compartments (from the 1st and 2nd order spectral peaks, enabling resolution of changes in dimension of ~1% in 1 μm structures). The ~1 μm Fourier spectral peak gives the average mitochondrial diameter, and the peak-width gives an index of the variability about the mean. It is important to consider whether the power of the harmonics contributed by certain birefringent bands of the sarcomere (i.e., at the Z- and M-lines) would interfere with the information provided by the primary ~0.95-1 μm spectral peak due to the regular pattern of mitochondria. It turns out that the mitochondrial optical contrast provides sufficient spectral power to the ~0.95-1 μm peak to far dominate that potentially contributed by the relatively small sarcomere-related signal. Evidence of this is provided by the observation that shifts in the ~0.95-1 μm spectral peak (Fig.S1, inset A) can be observed after Dz exposure without any change in the ~1.9-1.95 μm spectral peak (Fig.S1, inset B), ruling out significant changes in sarcomere spacing (or its contribution to the ~0.95-1 μm spectral peak) (Fig.S1).

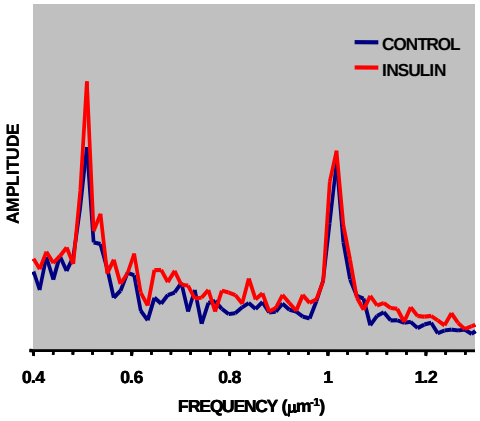

Figure S2c. Fourier analysis of mitochondrial size from TMRM loading: insulin (30 nM) exposure.

The transmitted optics linescan imaging protocol (using a 633 nm laser) described above was developed to examine relatively subtle changes in the dimensions of intracellular structures and organelles (i.e., mitochondria) both at high spatial and time resolution but without unwanted photochemical effects seen using wavelengths of light that are highly absorbed

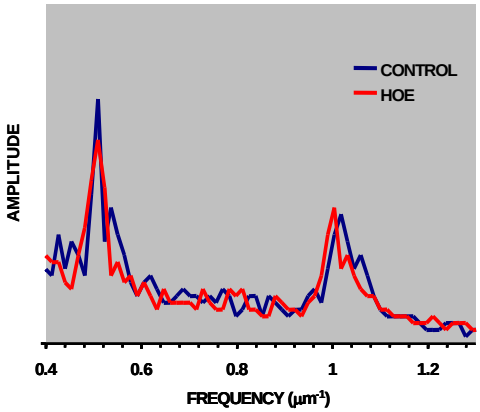

Figure S2d. Fourier analysis of mitochondrial size from TMRM loading: Hoe (10 μM) exposure.

by either endogenous or exogenous molecular species. On the other hand, imaging using wavelengths that are highly absorbed (and produce fluorescence) has the obvious advantage of an enhanced imaging contrast, and can confer structural specificity as well, but can significantly perturb cellular function (e.g., as demonstrated throughout the present work which combines the specificity of mitochondrial TMRM loading together with the photo-production of ROS causing MPT induction). In order to validate the present imaging protocol to assess changes in mitochondrial volume, we applied Fourier spectral analysis to X-Y frame scanned fluorescence confocal images of 125 nM TMRM loaded cardiac myocytes (using 543 nm laser excitation and LP570 emission, scanning 14.1 pixels/μm for 72.6 μm and 18.2 μm along the long and short cell axes, respectively, at 1 μm Z-resolution), which provides high contrast images of the periodic lattice of mitochondria arrayed within sarcomeres, *without significant contribution from non-mitochondrial structures*. Instead of the continuous imaging used in the transmitted protocol, only two such images were produced from each TMRM loaded cell to minimize photoexcitation: "Control" and at a time point 10 min later (as a 2nd Control, or after exposure to 10 μM HOE or 30 nM insulin; Fig. S2*a*). These images (Fig. S2*b*-*e*) yield the same pattern and resolution of long-axis

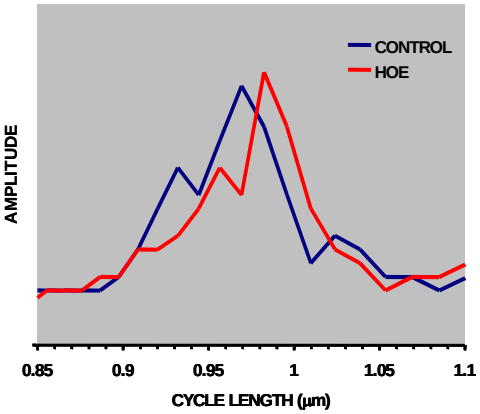

Figure S2e. Fourier analysis of mitochondrial size from TMRM loading: Hoe (10 μM) exposure. Enlargement of 2d order (mitochondrial) peak.

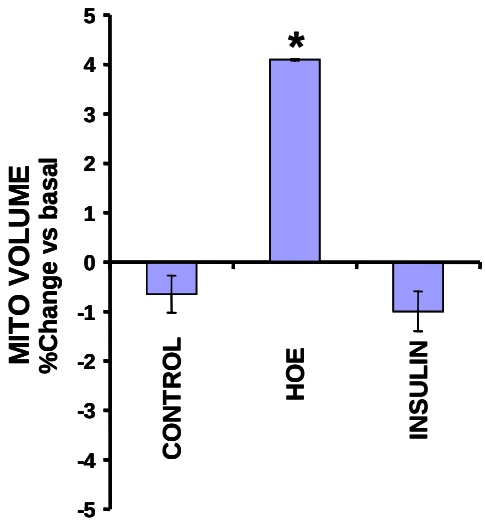

Figure S2f. Fourier analysis of mitochondrial size from TMRM loading: Summary comparison of Control, Hoe, and Insulin exposure. * $P < 0.001$.

spacing of the sarcomere and mitochondrial compartments (from the 1st and 2nd order Fourier spectral peaks, respectively) as obtained from the transmitted optics linescan imaging protocol, enabling resolution of changes in dimension of ~1% in 1 μm structures. Mitochondrial volume was estimated from the measured average mitochondrial diameter (from the 2nd order Fourier spectral peak) assuming spherical geometry. While Control imaging and insulin exposure (representative Fourier spectra in Figs. S2*b* and *c*, respectively) do not cause a significant change in mitochondrial dimension, HOE exposure causes an increase in diameter of ~0.013 μm (~4% volume swelling; see Fig. S2*d*,*e*). Figure S2*f* summarizes the results (cells obtained from 3 separate hearts, $n \geq 7$ observations per group) and shows that HOE produces a significant ~4% change in mitochondrial volume ($P<0.001$), whereas Control imaging and insulin do not have a significant effect on mitochondrial volume (P=ns). These results provide validation and agree in detail with that obtained using the transmitted optics linescan imaging protocol in Fig.4b-d from the main text.

SUPPLEMENT 2

Mitochondrial membrane potential: effect of hypoxia/reoxygenation

Cardiac myocytes loaded with TMRM (without DCF) were subjected to 1 hr hypoxia followed by rapid reoxygenation. The membrane potential was monitored measuring TMRM

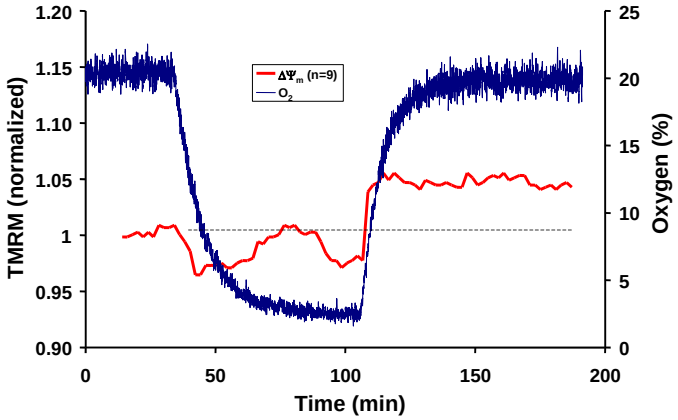

Figure S3. Mitochondrial membrane potential during Hypoxia/Reoxygenation.

fluorescence at two minute intervals during the hypoxia/reoxygenation protocol using a 10x/0.25 lens without optical zoom. After induction of hypoxia, cells become mildly depolarized (with some fluctuation noted during the hypoxic period); the cells become mildly hyperpolarized following the reoxygenation phase (figure S3; trace is average of n=9).

SUPPLEMENT 3

The role of mitoK$_{ATP}$ in protection signaling

In addition to diazoxide, pinacidil, which activates both mitochondrial and sarcolemmal K_{ATP} channels also enhances MPT ROS threshold in cardiac myocytes; this protection by pinacidil is fully inhibited by 100 μM 5HD (figure S4). Considerable attention has been paid to the role of the mitoK$_{ATP}$ as a key effector in protection, since it mimics many aspects of cardiac (and neuronal) ischemic preconditioning. The present results extend this idea to include the concept that the mitoK$_{ATP}$ is but one of multiple triggering mechanisms that produce regulatory mitochondrial swelling which in turn can mimic preconditioning. By the same logic, the mitoK$_{ATP}$ cannot be considered as an end effector in protection, as demonstrated in the present study.

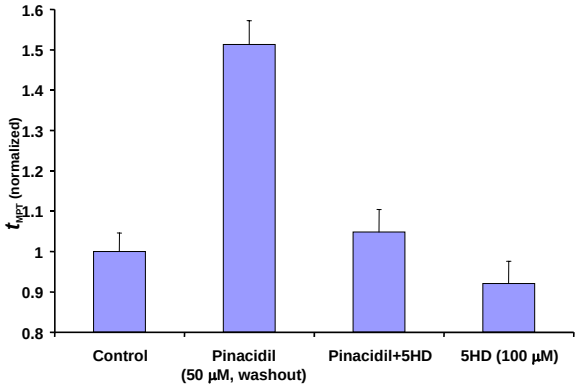

Figure S4. Cardioprotection induced by pinacidil requires the mitoK$_{ATP}$.

Interestingly, while Dz (and pinacidil (1)) causes flavoprotein oxidation (see figure 4b in main text, and figure S5), PMA does not (not shown). Furthermore, PMA shortens the

latency and increases the amplitude of the flavoprotein response to Dz (1). Similarly, Hoe and DADLE (δ-opioid)-mediated preconditioning are both PKC translocation-dependent and can be blocked by 5HD, and while they also produce *no* flavoprotein response, both shorten the latency and increase the flavoprotein response to Dz in a manner completely analogous to that seen with PMA (not shown). It deserves mention that while the flavoprotein response to Dz can reasonably be taken as a signal of mitoK$_{ATP}$ activity (1), based on the fact that the flavoprotein inhibitor, diphenyleneiodonium (DPI), can completely prevent this flavoprotein response *without* affecting the preconditioning action (i.e., MPT protection) of Dz (Fig. S5) argues that this phenomenon (and the function of the DPI-inhibited flavoproteins) is unrelated to the downstream mechanism of preconditioning.

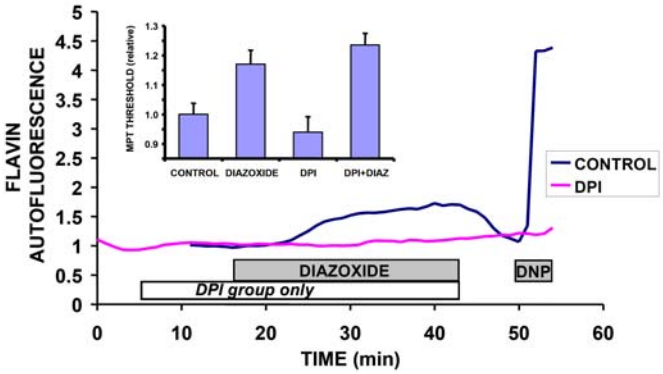

Figure S5. The mitoK$_{ATP}$-mediated decrease in susceptibility to ROS induction of the MPT is independent of flavoproteins.

SUPPLEMENT 4

Additional agents affecting protection; memory-associated vs memory-lacking protection signaling.

In addition to the array of distinct cardio/neuroprotective modulators presented in the main text (i.e., hypoxic preconditioning, Dz, HOE, DADLE, CSA, SFA, PMA, leptin, Li^+, SB (216763 & 415286), CCPA, bradykinin, GLP-1, IGF-1, insulin; also the pathway specific inhibitors including 5HD, BIS, NAC, IAA94, TMZ, LY 294002, Rp-8-CPT-cAMPS,

rapamycin, wortmannin (see main text for abbreviations)), the ability to exert protection through increasing the MPT ROS threshold has also been extended to include erythropoetin (figure S6), M_2 muscarinic, and α- and β-adrenergic stimulation (M.J. and S.J.S., unpublished data).

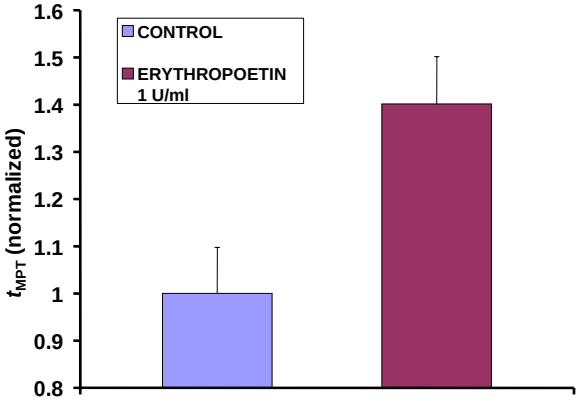

Figure S6. The effect of erythropoetin on MPT threshold in cardiac myocytes

Figure S7 shows evidence for the presence or absence of protection (t_{MPT}) "memory" exerted by swellers vs non-swellers, respectively. Protection by non-swellers, such as insulin and CCPA (and IGF-1, GLP-1, Li^+, and SB, not shown), is completely abolished by 15 min of washout, whereas the protection by swellers, such as Dz, Hoe, DADLE, SFA (and hypoxic PC, pinacidil, CSA, and bradykinin, not shown), is sustained at least through 1 hr of washout. Thus, swellers exhibit a memory of hours (i.e., each work as PC), and that of non-swellers do not have a significant memory.

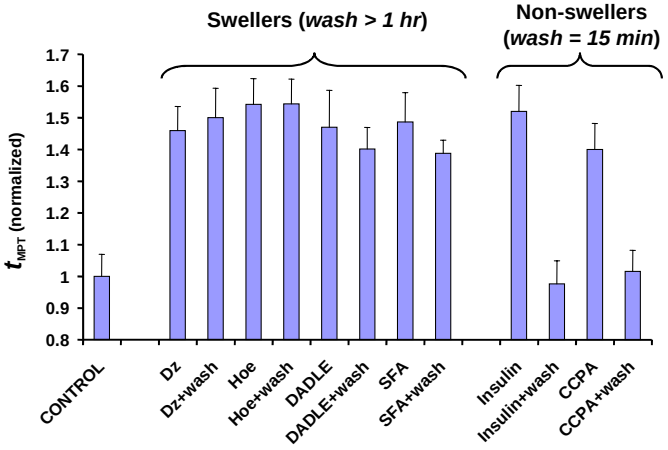

Figure S7. Cardioprotection Memory: Swellers vs Non-Swellers.

SUPPLEMENT 5

Effect of intracellular Ca^{2+} concentration on MPT induction in intact cardiac myocytes.

Mostly based on the results from experiments on isolated mitochondrial suspension, it was suggested that Ca^{2+} overload is an important factor that leads to onset of MPT (2, 3). We devised a set of experiments to evaluate the effect of intracellular Ca^{2+} concentration on MPT induction in intact cardiac myocytes. MPT ROS threshold during a "clamp" of intracellular Ca^{2+} >500nM for >20 min (using 10hz electrical tetanization in 5 mM bathing Ca^{2+} in the presence of thapsigargin or cyclopiazonic acid to disable the sarcoplasmic reticulum) was identical to that in unstimulated cells (with a cytoplasmic Ca^{2+} of ~100nM) (figure S8). Figure S9 shows the experimental demonstration of the tetanization technique in Indo-1 free acid loaded cardiac myocytes in 1, 2, and 5 mM bathing Ca^{2+} (4). However, skinning these same cardiac myocytes and maintaining them in carefully prepared Ca^{2+}/EGTA buffered solutions showed the following: 100 nM Ca^{2+} resulted in the same MPT ROS threshold as in intact

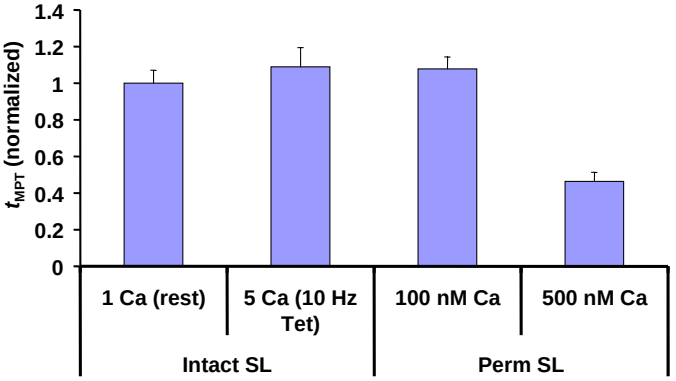

Figure S8. Role of Ca^{2+} in ROS induction of MPT in cardiac myocytes: intact vs permeabilized sarcolemma

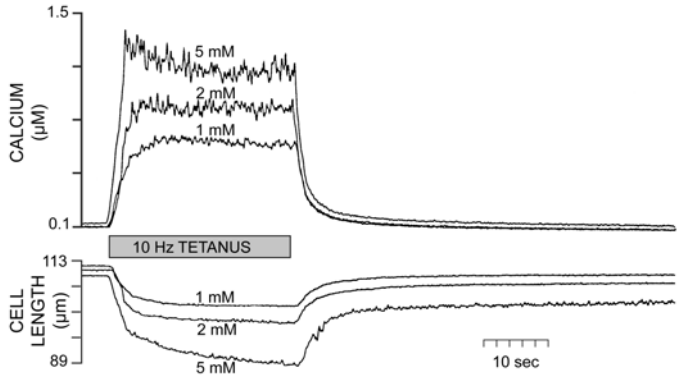

Figure S9. Tetanization of indo-1 free acid loaded cardiac myocytes in 1, 2, and 5 mM bathing Ca^{2+}.

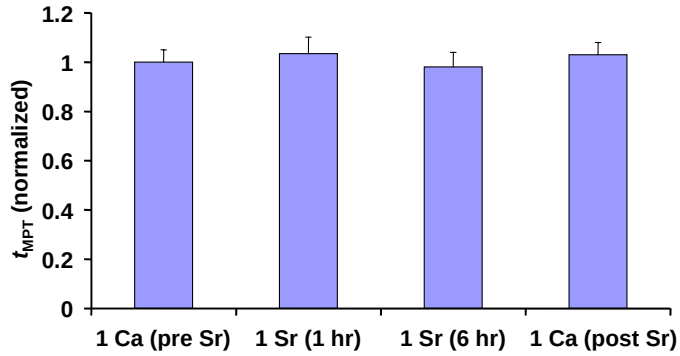

Figure S10. Role of Ca^{2+} in ROS induction of MPT in intact cardiac myocytes

cells; however, bathing skinned cells in 500 nM Ca^{2+} resulted in a decrease of MPT ROS threshold by more than half of that observed in 100 nM Ca^{2+} (figure S8). Thus, we speculate that once cardiac mitochondria are isolated from the cytoplasm some critical factor is lost such that the permeability transition pore complex now becomes susceptible to high Ca^{2+}. Furthermore, it has been shown that the Ca^{2+} sensitivity of MPT induction in isolated mitochondria is not reproduced by substitution of equimolar levels of Sr^{2+} (it requires more than an order of magnitude greater levels of Sr^{2+} than Ca^{2+} for MPT induction; see (5). We used this convenient property of Sr^{2+} to devise experiments in intact cells that would be essentially free of intracellular Ca^{2+}, with replacement by a divalent ion that does not cause MPT induction. Complete equimolar replacement of Ca^{2+} for Sr^{2+} (for 6 hours) in intact cardiac myocytes resulted in the *same* MPT ROS threshold as seen in cells with normal Ca^{2+} (figure S10). Thus Ca^{2+} probably does not play an important role in mediating MPT induction in intact cardiac myocytes. MPT ROS threshold measurements after replacement and restoration of normal Ca^{2+} to these Sr^{2+}-treated cells was comparable to the initial controls (figure S10).

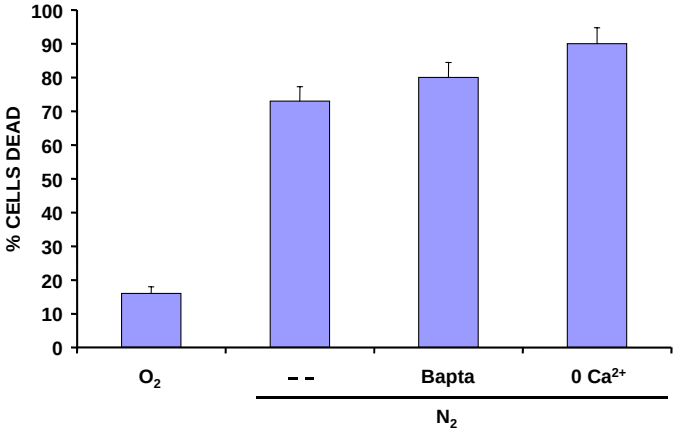

Figure S11. Role of Ca^{2+} in cardiac myocyte death after hypoxia/reoxygenation

Figure S11 demonstrates that buffering intracellular Ca^{2+} (with bapta) or limiting Ca^{2+} influx (in nominally Ca^{2+}-free buffer) does not limit cardiac myocyte death after hypoxia/reoxygenation.

Supplemental References

1. Sato, T., O'Rourke, B., and Marban, E. 1998. Modulation of mitochondrial ATP-dependent K+ channels by protein kinase C. *Circ. Res.* **83**:10-114.

2. Halestrap, A.P. 1999. The mitochondrial permeability transition: its molecular mechanism and role in reperfusion injury. *Biochem. Soc. Symp*. **66**:181-203.

3. Kowaltowski, A.J., Castilho, R. F., and Vercesi, A.E. 2001. Mitochondrial permeability transition and oxidative stress. *FEBS Letters* **495**:12-15.

4. Sollott, S.J., Ziman, B.D., and Lakatta, E.G. 1992. Novel technique to load indo-1 free acid into single adult cardiac myocytes to assess cytosolic Ca2+. *Am J Physiol.* **262**:H1941-H1949.

5. Hunter, D.R., Haworth, R.A., and Southard, J.H. 1976. Relationship between configuration, function, and permeability in calcium-treated mitochondria. J*. Biol. Chem*. **251**:5069-5077.